Nanoscale Res Lett (2009) 4:70–77
DOI 10.1007/s11671-008-9204-7

NANO EXPRESS

The Effect of Iron Oxide Magnetic Nanoparticles on Smooth Muscle Cells

Song Zhang · Xiangjian Chen · Chunrong Gu · Yu Zhang · Jindan Xu · Zhiping Bian · Di Yang · Ning Gu

Received: 17 September 2008 / Accepted: 29 October 2008 / Published online: 2 December 2008

Abstract Recently, magnetic nanoparticles of iron oxide (Fe_3O_4, γ-Fe_2O_3) have shown an increasing number of applications in the field of biomedicine, but some questions have been raised about the potential impact of these nanoparticles on the environment and human health. In this work, the three types of magnetic nanoparticles (DMSA-Fe_2O_3, APTS-Fe_2O_3, and GLU-Fe_2O_3) with the same crystal structure, magnetic properties, and size distribution was designed, prepared, and characterized by transmission electronic microscopy, powder X-ray diffraction, zeta potential analyzer, vibrating sample magnetometer, and Fourier transform Infrared spectroscopy. Then, we have investigated the effect of the three types of magnetic nanoparticles (DMSA-Fe_2O_3, APTS-Fe_2O_3, and GLU-Fe_2O_3) on smooth muscle cells (SMCs). Cellular uptake of nanoparticles by SMC displays the dose, the incubation time and surface property dependent patterns. Through the thin section TEM images, we observe that DMSA-Fe_2O_3 is incorporated into the lysosome of SMCs. The magnetic nanoparticles have no inflammation impact, but decrease the viability of SMCs. The other questions about metabolism and other impacts will be the next subject of further studies.

Keywords Magnetic nanoparticles · Iron oxide · Smooth muscle cells · Cellular uptake · Viability

Introduction

Magnetic nanomaterial has shown an increasing number of applications in different fields of information, mechanics, and biomedicine due to their multifunctional properties such as small size effect, superparamagnetism, inherently biocompatibility, etc. [1–4]. Especially in the last decade, the field of biomedicine witnessed an explosion of interest in the use of magnetic nanomaterial in earlier diagnosis and effective treatment of some diseases, such as magnetic resonance imaging (MRI) [5, 6], drug delivery [7–11], hyperthermia, etc. [12, 13]. In MRI, magnetic nanoparticles serve as contrast enhancement agents, in drug delivery, they function as drug carriers delivering and releasing the drug into target cells, while in hyperthermia, they serve as generator of heat under alternating current magnetic field. In certain cases, the employment based on magnetic nanomaterial has displayed significant advantages over conventional material with regard to assay sensitivity, effect of treatment, side effect, etc.

In biological applications, the current magnetic nanoparticles (MNPs) of iron oxide (Fe_3O_4, γ-Fe_2O_3) may be modest and biocompatible [14, 15], but some questions have been raised about the potential impact of these nanoparticles on the environment and human health. Numerous investigations have been carried out using iron oxides nanoparticles linked to their high mobility and specific reactivity with cells. Some results indicate that iron

Song Zhang and Xiangjian Chen contributed equally to this work.

S. Zhang · Y. Zhang · N. Gu (✉)
State Key Laboratory of Molecule and Biomolecule Electronics, Jiangsu Provincial Laboratory for Biomaterials and Devices, Southeast University, 210096 Nanjing, People's Republic of China
e-mail: guning@seu.edu.cn

X. Chen · C. Gu · J. Xu · Z. Bian · D. Yang (✉)
Institute of Cardiovascular Disease, The First Affiliated Hospital of Nanjing Medical University, 210029 Nanjing, People's Republic of China
e-mail: dyang@public1.ptt.js.cn

oxide nanoparticles could be internalized by cells and induce a dramatic decrease in the metabolic activity and proliferation of human cells (MSTO-211H) [16–20]. A quantifiable model cell system shows that intracellular delivery of even moderate levels of iron oxide (Fe_2O_3) nanoparticles may adversely affect cell function. More specifically, the cytotoxicity studies show that exposure to increasing concentrations of anionic MNPs, from 0.15 to 15 mM of iron, results in a dose-dependent diminishing viability and capacity of PC12 cells to extend neurites in response to nerve growth factor [21].

Recently, the cytotoxicity assessment about iron oxide nanoparticles has been focused on by more and more researchers. Nevertheless, as mentioned by Auffan et al. [16], toxicological data are difficult to compare since the parameters controlled in each of these studies may differ. These parameters involve size distribution, surface properties, magnetic properties, stability in biological media, etc. In this present study, the aim is to elucidate the effect of different iron oxide magnetic nanoparticles (γ-Fe_2O_3, MNPs) on Sprague-Dawley rat smooth muscle cell (SMC) in vitro. In particularly, MNPs were coated by meso-2, 3-dimercaptosuccinic acid (DMSA), 3-amino-propyltriethoxysilane (APTS), and L-glutamic acid (GLU), respectively, but possess the same size distribution and magnetic properties and stability, which can ensure the consistence and comparability of investigation results.

Experimental Section

Reagents

Magnetic nanoparticles were synthesized, and stored in the dark at 4 °C. Dulbecco's modified Eagle's medium (DMEM) was purchased from GIBCO Company. Penicillin and streptomycin were purchased SIGMA Company. TNF-α ELISA Kit was purchased from BOSTER Company. All of other chemicals were of reagent grade and were used as received without further purification. Double distilled water was used for all the experiments.

Preparation of the Coated MNPs

Fe_3O_4 nanoparticles were synthesized by chemical coprecipitation of Molday [22]. Typically, a solution of mixture of $FeCl_3$ and $FeSO_4$ (molar ratio 2:1) was prepared under N_2 protecting, followed by the slow addition of enough ammonia aqueous solution with vigorous stirring for 30 min. The black Fe_3O_4 precipitates were obtained and washed immediately with distilled water for five times by magnetic separation. The final precipitates were dispersed in distilled water with concentration of 0.128 M and pH 3.0, and oxidized into more stable MNPs (γ-Fe_2O_3) by air at the temperature of 90 °C.

According to the process described in the literature [23, 24], MNPs were coated with DMSA and GLU. Finally stable aqueous sol DMSA-MNPs (DMSA-Fe_2O_3), and GLU-MNPs (GLU-Fe_2O_3) were obtained. Similarly, APTS-MNPs (APTS-Fe_2O_3) were prepared according to literature [25]. The part of above samples was dried into powder at room temperature under vacuum.

Characterization

The particle size and morphology of the coated MNPs was determined by transmission electronic microscopy (TEM, JEOL, JEM-200EX). Powder X-ray diffraction (XRD, Rigaku, D/Max-RA, $\lambda = 1.5405 \times 10^{-10}$ m, CuK) was used to determine the crystal structure of MNPs. Surface charge measurements were performed with a zeta potential analyzer (BECKMAN, Delsa 440SX). The magnetic measurements were carried out with a vibrating sample magnetometer (VSM, Lakeshore 7407). Fourier transform infrared (FTIR) spectroscopy measurements were performed on a Bruker Fourier transform spectrometer model VECTOR22 using KBr pressed discs.

Cell Culture

Sprague-Dawley (SD) rat aortic SMCs were grown from explants of normal SD rat aorta fragments. Cells were further cultured in Dulbecco's modified Eagle medium (DMEM) containing 15% fetal bovine serum (FBS), penicillin (100 μg/mL), and streptomycin (100 μg/mL), in 5% CO_2 chamber.

Incubation of SMC with the Coated MNPs

All the coated MNPs was sterilized with filter-film (pore size, 0.22 μm) and sonicated before dilution into DMEM culture medium to ensure even particle suspension. Then, the MNPs were diluted with DMEM at different concentration and added into the plates in triplicate for a further specified time after the normal medium was removed. All control cells were cultured in the absence of any particles. Every experiment was repeated at least three times independently.

Cellular Uptake of MNPs Assay

Cellular uptake of MNPs was evaluated according to the method of Petri-Fink [26]. The supernate of cells on the 6-well plates was removed and cells were thoroughly washed with PBS and resuspended in 2 M HCl (1 mL/well of a 6-well plate) at 37 °C for 2 h. The protein concentration of

mixture was determined at 280 nm by Ultraviolet Visible Spectrophotometer (UV–vis). 1 mL of 5% solution of $K_4[Fe(CN)_6]$ in H_2O was added, and the absorbance of samples was read after 10 min at 690 nm. A standard curve of an aqueous $FeCl_3 \cdot 6H_2O$ solution was treated in the same conditions to quantify the amount of cellular uptake of MNPs. The cellular uptake of MNPs was expressed at the amount of Fe_2O_3 (weight, μg) per milligram of protein.

TEM Analysis

The SMC incubated with DMSA-MNPs for 24 h were washed with PBS and fixed in 4% glutaraldehyde solution for 1 h at 4 °C. The cells were postfixed in 1% osmium tetroxide for 1 h at room temperature and washed. Then, cells were scraped and concentrated in 2.5% agar in 0.05 M cacodylate buffer. The obtained samples were then treated with 2% uranyl acetate solution for 1 h and subsequently dehydrated by means of ethanol/water solutions, with increasing ethanol content and embedded in epoxy resin [27]. The samples were cut at 70 nm (ultrathin sections) with an ultramicrotome. Ultrathin sections were transferred to the 300 mesh copper grid and stained with 5% uranyl acetate. The copper grid was observed on a transmission electron microscope (TEM, HITACHIH-600) at 80 kV.

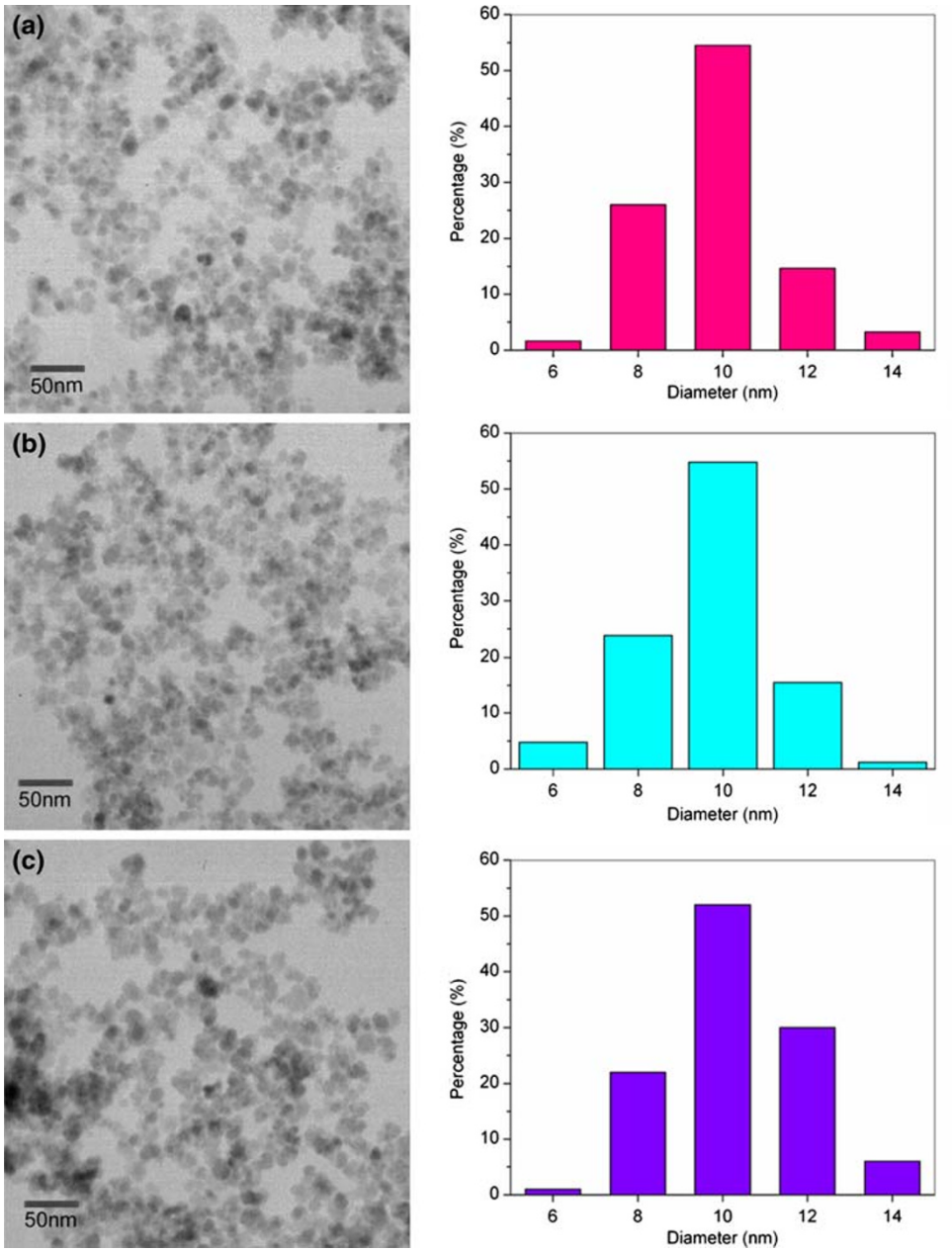

Fig. 1 The TEM image and size distribution of nanoparticles. **a** DMSA-MNPs, **b** APTS-MNPs, and **c** GLU-MNPs

TNF-α Assay

After incubation for a period of time, cell culture supernate was collected and centrifuged at 8,000×*g* for 30 min to remove cell debris and nanoparticles. Tumor necrosis factor α (TNF-α) protein concentrations in the supernate were measured using an ELISA kit (RAT TNF-α, ELISA KIT, BOSTER) according to the manufacturer's instructions.

Cell Viability Assay

Viability of SMC was determined by using MTT (3-(4,5-dimethylthiazol-2-yl)-2,5-diphenyltetra-zolium bromide) assay. After incubation the supernate was removed and 200 μL MTT solution (0.5 mg/mL in DMEM medium) was added at 37 °C for 2 h. Then, cells were rinsed two times with PBS and 150 μL extracting solution (0.04 M HCl in isopropanol) was added to each well of 96-well plates. The plates were placed for 15 min at ambient temperature to dissolve the dyes and the dye extract was transferred to 96 well Elisa plates. Absorbance was assayed at 570 nm by Ultra Microplate Reader ELX808 IU (Bio-Tek) and the cell viability was expressed in percent based on the control.

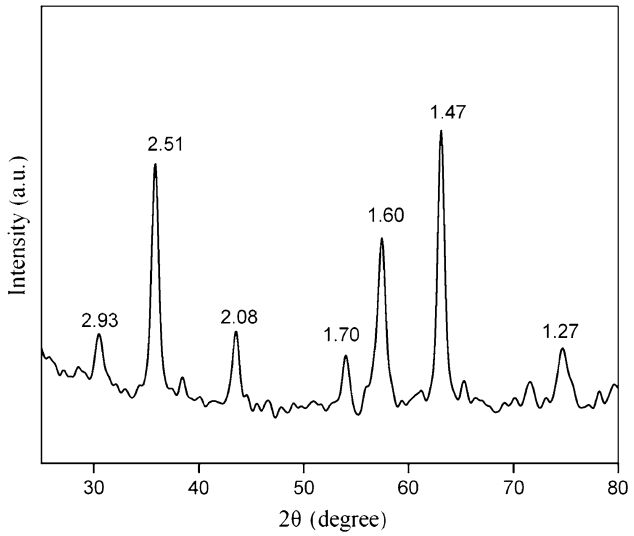

Fig. 2 X-ray powder diffraction of the uncoated MNPs

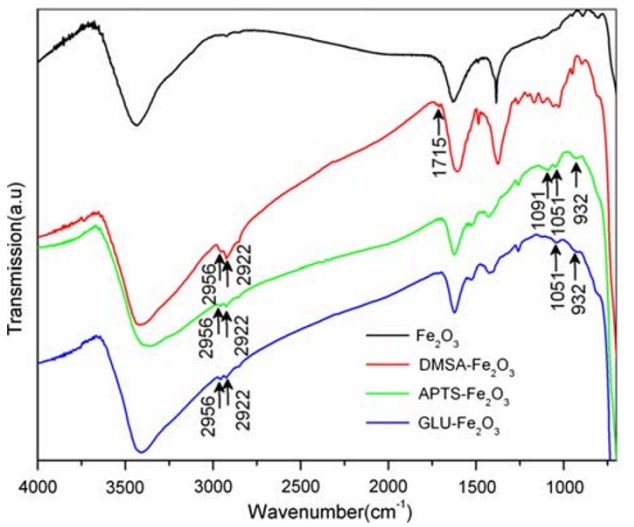

Fig. 3 FTIR spectra of the uncoated MNPs, DMSA-MNPs, APTS-MNPs, and GLU-MNPs

Results and Discussion

Preparation of the Coated MNPs and Characterization

Magnetic nanoparticles were synthesized by chemical coprecipitation and stable magnetic fluid was obtained via coating by DMSA, APTS, and GLU. The morphology and

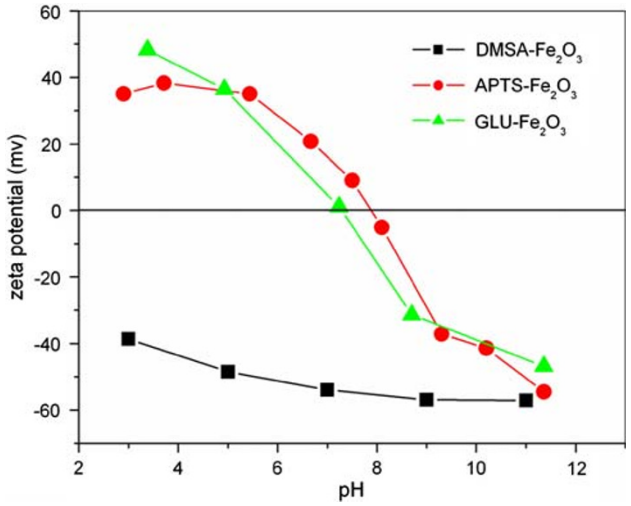

Fig. 4 pH-dependent zeta potential curves of DMSA-MNPs, APTS-MNPs, and GLU-MNPs

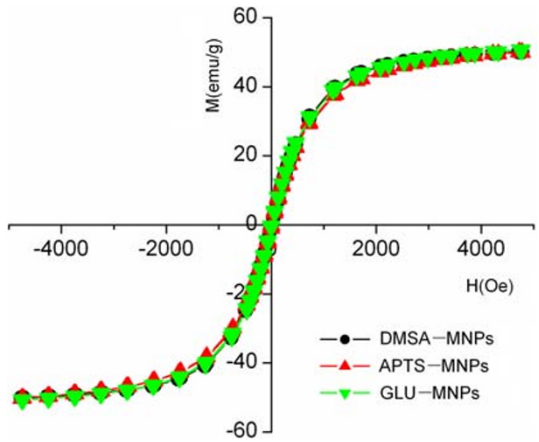

Fig. 5 Magnetization versus applied magnetic field for the coated MNPs

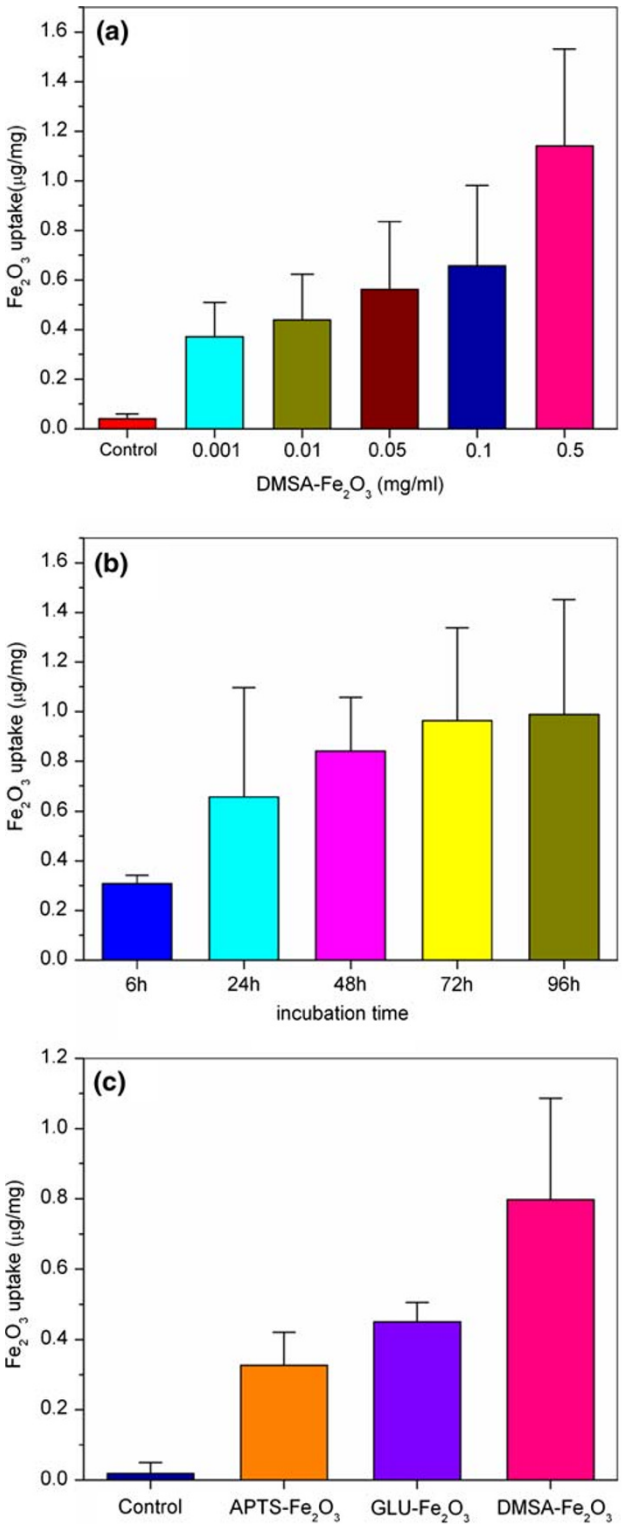

Fig. 6 Cellular uptake of MNPs by smooth muscle cell (SMC). All values are represented the mean ± standard deviation (SD) of three experiments, each performed in triplicate. Control columns mean that SMC was incubated with only DMEM. **a** SMC was incubated with DMEM containing the indicated concentration of DMSA-MNPs for 24 h. **b** SMC was incubated with DMEM containing 0.1 mg/mL DMSA-MNPs for the indicated incubation time, and **c** SMC was incubated with DMEM containing 0.1 mg/mL indicated MNPs for 24 h

structure of particles were observed by TEM, and the images indicate that most of the particles are quasi-spherical and with an average diameter of 10 nm. The TEM image and size distribution of particles are shown in Fig. 1 The same morphology and size distribution can avoid the difference of size effect. The phase identification of the uncoated MNPs was performed by XRD. As shown in Fig. 2, the result shows that the MNPs are inverse cubic spinel structure [28]. Compared with the theoretical values, the reduction of d-spacing obtained experimentally is due to the lattice constrictions for nanosized particles [25].

Fourier transform infrared spectroscopy was used to confirm that the DMSA, APTS, and GLU were successfully coated on the nanoparticles. The FTIR spectra of MNPs, DMSA-MNPs, APTS-MNPs, and GLU-MNPs are shown in Fig. 3 All samples show broad band at 3400 cm^{-1} indicative of the presence of –OH groups on nanoparticles surface. Compared with the uncoated MNPs, all the coated MNPs possess absorption bands in 2956 and 2922 cm^{-1} due to stretching vibration of C–H bond. In addition, for DMSA-MNPs, the band in 1715 cm^{-1} appears due to stretching vibration of C=O bond, which reveals the existence of DMSA. For APTS-MNPs, bands in 1091 and 1051 cm^{-1} are attributed to stretching vibration of C–N bond and Si–O bond, band in 932 cm^{-1} is attributed to bending vibration of $–NH_2$. In the spectrum of GLU-MNPs, the bands in 1091 and in 932 cm^{-1} are also observed because the existence of C–O and $–NH_2$ group, which is the strong evidence that GLU is bonded to the surface of the nanoparticles.

Zeta (ξ) potential measurement as a function of pH has been performed to confirm the surface charge properties and the presence of DMSA, APTS, and GLU on the surface of MNPs. Figure 4 shows that the DMSA-MNPs have high negative potential at the pH range, while the APTS and GLU-MNPs are positively charged at lower pH and negatively at higher pH and their isoelectric points (IEP) are 7.2 and 7.9, respectively. The difference of charge properties of them attribute to the ionization of the functional groups, such as –COOH, –SH and $–NH_2$ at different pH. According to results, we can make sure that the surface charge property is negative for DMSA-MNPs, positive for APTS-MNPs, and nearly neutral for GLU-MNPs in the physicochemical states (pH 7.4).

The magnetic property of the MNPs was measured by VSM. Figure 5 shows the magnetization of the coated MNPs as a function of an external field at ambient temperature. The three of MNPs possess similar magnetization loops and saturation magnetization (50 emu/g) because of

the same structure and size distribution. The synthesized MNPs also show a superparamagnetic behavior, as evidenced by zero coercivity and remanance on the magnetization loops.

Cellular Uptake of MNPs

The cellular uptake amount is counted based on the Fe_2O_3 per milligram protein that released from the cells. For the DMSA-MNPs, the cellular uptake of MNPs by SMC increases with increasing concentration from 0.001 to 0.5 mg/mL in DMEM, as shown in Fig. 6a. The uptake also shows the same behavior with increasing of incubation time from 24 to 72 h when the concentration of DMSA-MNPs is 0.1 mg/mL (Fig. 6b). Briefly, the cellular uptake shows a clear dose and incubation time dependent patterns under the experiment conditions.

The cellular uptake indicates a function of surface properties of MNPs. From Fig. 6c, there is obvious difference among the three types of MNPs at the same concentration (0.1 mg/mL) for the same incubation time (24 h). The uptake amount of APTS-MNPs, GLU-MNPs, and DMSA-MNPs are 3.72, 4.60, and 8.98 μg per milligram protein, respectively. We infer that the different surface properties, such as charges of surface molecules, result in the different affinity with SMC [27, 29–32]. According to the results, it is promising to facilitate or alter uptake of SMC by altering the surface properties of MNPs.

Endocytosis of DMSA-MNPs by SMC

The thin section TEM images indicate that the DMSA-MNPs are incorporated into SMC after 24 h of incubation at 0.1 mg/mL of concentration. As shown in Fig. 7, the MNPs are clearly visible and distinct from the cellular matter because of their high electron density. The particles or their aggregates are distributed outside, on the surface of

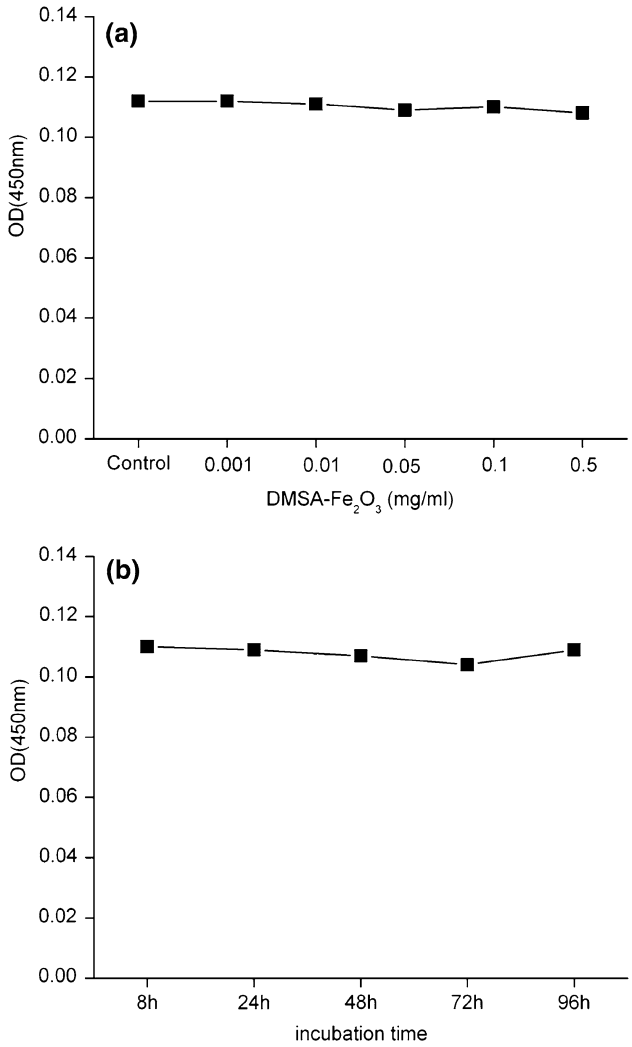

Fig. 8 The TNF-α level in the supernate of SMC incubated with DMSA-MNPs. The level is expressed with optical density of ELISA results. **a** SMC was incubated with DMEM containing the indicated concentration of DMSA-MNPs for 24 h. **b** SMC was incubated with DMEM containing 0.1 mg/mL DMSA-MNPs for the indicated incubation time

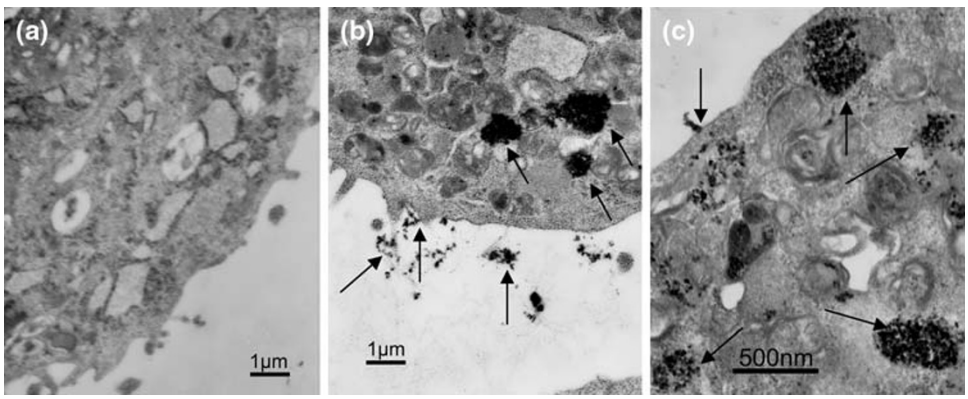

Fig. 7 The thin-section TEM images of SMC incubated with 0.1 mg/mL of DMSA-MNPs for 24 h. **a** Control SMC × 10 K, **b** SMC incubated with DMSA-MNPs × 10 K, and **c** SMC incubated with DMSA-MNPs × 35 K. Arrows denote the MNPs or their aggregates

the membrane and inside of cell. We infer that the nanoparticles or their aggregates are absorbed on the membrane due to their small size effect, and incorporated by endocytosis vesicles through the deformation of the membrane, and then dispersed in cytoplasm of SMC. We can observe that the particles are swallowed by lysosome in cytoplasm from Fig. 7b and c. However, the fate of MNPs during cellular degradation is a key and unknown question.

TNF-α Level

Tumor necrosis factor α is a polypeptide cytokine that promotes antitumor and immune responses [33], also called pro-inflammatory cytokine. For SMC, TNF-α is released from cells when the cells are damaged, and then the free TNF-α will promote the inflammatory damage of cells inversely. The supernate of SMC incubated with DMSA-MNPs under the same experiment conditions was collected and mixed. Then, the TNF-α was assayed by ELISA. The results were shown in Fig. 8 The level of TNF-α is normal compared with control, which means that DMSA-MNPs did not elicit the production of the pro-inflammatory cytokine TNF-α. Therefore, DMSA-MNPs cannot lead to SMC inflammatory damage in vitro. The other two types of MNPs show the same results (the data not shown). In conclusion, the three types of MNPs display the biocompatibility with SMC. Using our chosen endpoints, SMC do not damaged by the MNPs.

SMC Viability/Cytotoxicity Studies

The MTT (3-(4,5-dimethylthiazol-2-yl)-2,5-diphenyltetrazolium bromide) assay is a simple nonradioactive colorimetric assay to measure cell cytotoxicity, proliferation, or viability [34]. The active SMC is able to convert this dye into a water-insoluble dark-blue formazan by reductive cleavage of the tetrazolium ring [35]. Formazan crystals, then, was dissolved in acidification isopropanol by measuring the absorbance of the solution at 570 nm, and the resultant value is related to the number of living cells.

The viability of SMC is apparently decreased with the increasing of the concentration and incubation time of DMSA-MNPs compared with the control, as shown in Fig. 9a and b. The data were analyzed by statistical method and the result indicates there is statistical difference when the concentration of magnetic nanoparticles is more than 0.1 mg/mL ($p < 0.05$). Here, the viability means the activity, the cytotoxicity and the number of SMC. The decrease of viability may be resulted from the damage, proliferation inhibition of SMC by DMSA-MNPs.

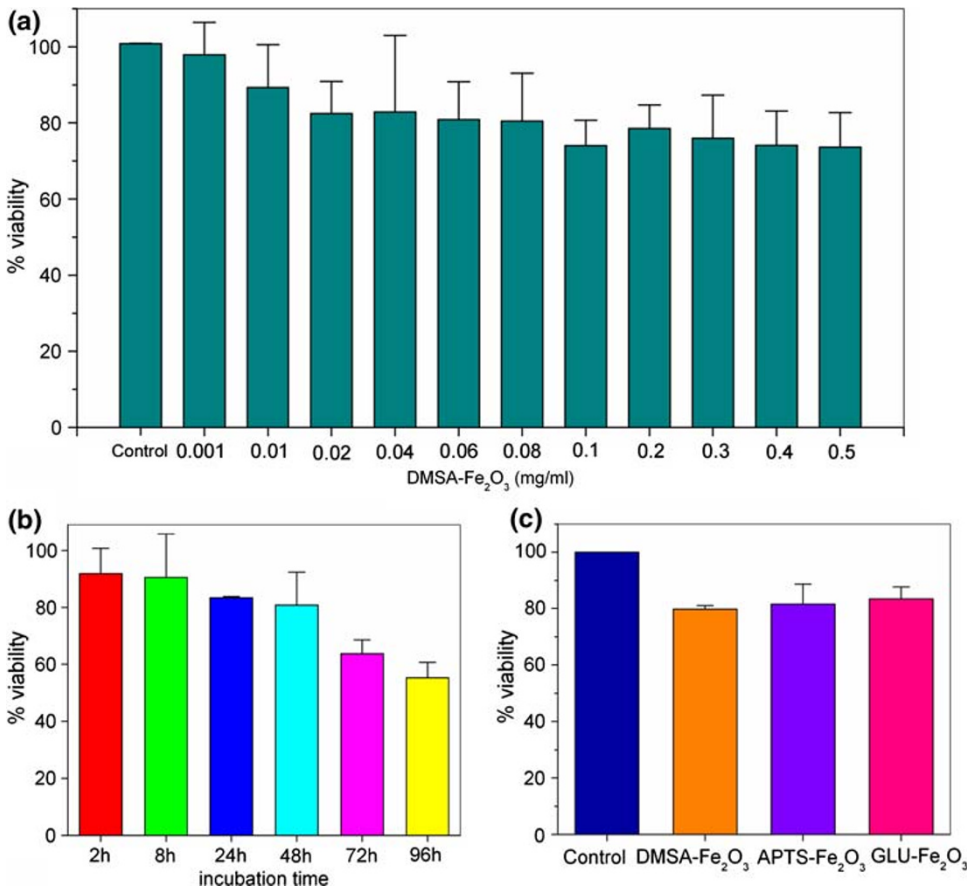

Fig. 9 The viability of SMC incubated with MNPs. All values are expressed as the mean ± (SD) of three experiments, each performed in octuple. Control columns mean that SMC was incubated with only DMEM. **a** SMC was incubated with DMEM containing the indicated concentration of DMSA-MNPs for 24 h. **b** SMC was incubated with DMEM containing 0.1 mg/mL DMSA-MNPs for the indicated incubation time. **c** SMC was incubated with DMEM containing 0.1 mg/mL indicated MNPs for 24 h

Considering the TNF-α level, we can infer that the decrease of viability is caused from proliferation inhibition of SMC by DMSA-MNPs.

However, the viability of SMC has not shown obviously statistical difference when incubated with three types of MNPs at the same concentration (0.1 mg/mL) and incubation time (24 h), which demonstrates that the properties of MNPs (used in the experiments) hardly have effect on the viability of SMC. The data are shown in Fig. 9c.

Conclusions

The work has focused on the effect of iron oxide magnetic nanoparticles on SMCs. The magnetic nanoparticles (DMSA-MNPs APTS-MNPs, and GLU-MNPs) have the same crystal structure, magnetic properties, and size distribution. Cellular uptake of MNPs displays the dose, the incubation time, and surface property dependent patterns. Through the thin section TEM images, we observe that DMSA-MNPs are incorporated into the lysosome of SMC. The MNPs have no inflammation impact, but decrease the viability of SMC. The other questions about metabolism and other impacts will be the next subject of further studies.

Acknowledgments The authors gratefully acknowledge the support of National Natural Science Foundation of China (No. 60571031, 60501009 90406023, 30570745, and 30772781), National Basic Research Program of China (No. 2006CB933206 and 2006CB705606), and the fund of Key Laboratory of Jiangsu Province (XK200705).

References

1. C. Sjögren, C. Johansson, A. Naevestad, P. Sontum, K. Briley-Saebo, A. Fahlvik, Magn. Reson. Imaging **15**, 55 (1997). doi:10.1016/S0730-725X(96)00335-9
2. J. Roger, J.N. Pons, R. Massart, A. Halbreich, J.C. Bacri, Eur. Phys. J. Appl. Phys. **5**, 321 (1999). doi:10.1051/epjap:1999144
3. J.M. Perez, T. O'Loughin, F.J. Simeone, R. Weissleder, L. Josephson, J. Am. Chem. Soc **124**, 2856 (2002). doi:10.1021/ja017773n
4. A. Dyal, K. Loos, M. Noto, S.W. Chang, C. Spagnoli, K.V.P.M. Shafi et al., J. Am. Chem. Soc **125**, 1684 (2003). doi:10.1021/ja021223n
5. O. Veiseh, C. Sun, J. Gunn, N. Kohler, P. Gabikian, D. Lee et al., Nano Lett. **5**, 1003 (2005). doi:10.1021/nl0502569
6. Y.W. Jun, Y.M. Huh, J.S. Choi, J.H. Lee, H.T. Song, S. Kim et al., J. Am. Chem. Soc **127**, 5732 (2005). doi:10.1021/ja0422155
7. C. Alexiou, W. Arnold, R.J. Klein, F.G. Parak, P. Hulin, C. Bergemann, Cancer Res. **60**, 8 (2000)
8. M. Song, R.Y. Zhang, Y.Y. Dai, F. Gao, H.M. Chi, G. Lv et al., Biomaterials **27**, 4230 (2006). doi:10.1016/j.biomaterials.2006.03.021
9. R.Y. Zhang, X.M. Wang, C.H. Wu, M. Song, J.Y. Li, G. Lv et al., Nanotechnology **17**, 3622 (2006). doi:10.1088/0957-4484/17/14/043
10. J. Dobson, Drug Dev. Res. **67**, 55 (2006). doi:10.1002/ddr.20067
11. S. Dandamudi, R.B. Campbell, Biomaterials **28**, 4673 (2007). doi:10.1016/j.biomaterials.2007.07.024
12. A. Ito, M. Shinkai, H. Honda, T. Kobayashi, Cancer Gene Ther. **8**, 649 (2001). doi:10.1038/sj.cgt.7700357
13. M. Kawashita, M. Tanaka, T. Kokubo, Y. Inoue, T. Yao, S. Hamada et al., Biomaterials **26**, 2231 (2005). doi:10.1016/j.biomaterials.2004.07.014
14. A. Gojova, B. Guo, R.S. Kota, J.C. Rutledge, I.M. Kennedy, A.I. Barakat, Environ. Health Perspect. **115**, 403 (2007)
15. K. Muller, J.N. Skepper, M. Posfai, R. Trivedi, S. Howarth, C. Corot et al., Biomaterials **28**, 1629 (2007). doi:10.1016/j.biomaterials.2006.12.003
16. M. Auffan, L. Decome, J. Rose, T. Orsiere, M. De Meo, V. Briois et al., Environ. Sci. Technol. **40**, 4367 (2006). doi:10.1021/es060691k
17. S.K. Sahoo, V. Labhasetwar, Drug Discov. Today **8**, 1112 (2003). doi:10.1016/S1359-6446(03)02903-9
18. A. Halbreich, J. Roger, J.N. Pons, D. Geldwerth, M.F. Da Silva, M. Roudier et al., Biochimie **80**, 379 (1998). doi:10.1016/S0300-9084(00)80006-1
19. A.K. Gupta, M. Gupta, Biomaterials **26**, 3995 (2005). doi:10.1016/j.biomaterials.2004.10.012
20. A.K. Gupta, M. Gupta, Biomaterials **26**, 1565 (2005). doi:10.1016/j.biomaterials.2004.05.022
21. T.R. Pisanic, J.D. Blackwell, V.I. Shubayev, R.R. Finones, S. Jin, Biomaterials **28**, 2572 (2007). doi:10.1016/j.biomaterials.2007.01.043
22. R.S. Molday, US Patent 4452773 (1984)
23. N. Fauconnier, J.N. Pons, J. Roger, A. Bee, J. Colloid Interf. Sci. **194**, 427 (1997)
24. N. Fauconnier, A. Bee, J. Roger, J.N. Pons, J. Mol. Liq. **83**, 233 (1999). doi:10.1016/S0167-7322(99)00088-4
25. M. Ma, Y. Zhang, W. Yu, H.Y. Shen, H.Q. Zhang, N. Gu, Colloid Surf. A **212**, 219 (2003). doi:10.1016/S0927-7757(02)00305-9
26. A. Petri-Fink, M. Chastellain, L. Juillerat-Jeanneret, A. Ferrari, H. Hofmann, Biomaterials **26**, 2685 (2005). doi:10.1016/j.biomaterials.2004.07.023
27. F. Sonvico, S. Mornet, S. Vasseur, C. Dubernet, D. Jaillard, J. Degrouard et al., Bioconjug. Chem. **16**, 1181 (2005). doi:10.1021/bc050050z
28. H. Fang, C.Y. Ma, T.L. Wan, M. Zhang, W.H. Shi, J. Phys. Chem. C **111**, 1065 (2007). doi:10.1021/jp0672048
29. J.K. Zhou, C. Leuschner, C. Kumar, J.F. Hormes, W.O. Soboyejo, Biomaterials **27**, 2001 (2006). doi:10.1016/j.biomaterials.2005.10.013
30. K.M.K. Selim, Y.S. Ha, S.J. Kim, Y. Chang, T.J. Kim, G.H. Lee et al., Biomaterials **28**, 710 (2007). doi:10.1016/j.biomaterials.2006.09.014
31. K. Sou, B. Goins, S. Takeoka, E. Tsuchida, W.T. Phillips, Biomaterials **28**, 2655 (2007). doi:10.1016/j.biomaterials.2007.01.041
32. T.H. Chung, S.H. Wu, M. Yao, C.W. Lu, Y.S. Lin, Y. Hung et al., Biomaterials **28**, 2959 (2007). doi:10.1016/j.biomaterials.2007.03.006
33. M.B. Reid, Y.P. Li, Respir. Res. **2**, 269 (2001). doi:10.1186/rr67
34. A.K. Gupta, C. Berry, M. Gupta, A. Curtis, IEEE Trans. Nanobiosci. **2**, 255 (2003). doi:10.1109/TNB.2003.820279
35. T. Mosmann, J. Immunol. Methods **95**, 9 (1993)